Journal of Inorganic Biochemistry 193 (2019) 166–172

Contents lists available at ScienceDirect

Journal of Inorganic Biochemistry

journal homepage: www.elsevier.com/locate/jinorgbio

Facile synthesis of novel carbon-dots/hemin nanoplatforms for synergistic photo-thermal and photo-dynamic therapies

Wei Yang[c], Bing Wei[b], Zheng Yang[a,*], Liangquan Sheng[a,*]

[a] School of Chemistry and Materials Engineering, Fuyang Normal University, Fuyang 236037, PR China
[b] Biology and Food Engineering School, Fuyang Normal University, Fuyang 236037, PR China
[c] Anhui Chemical Engineering School, Anqing 246300, PR China

ARTICLE INFO

Keywords:
Enhanced photo-thermal therapy
Photo-dynamic therapy
FRET effect
Dual-modal nanoplatform
Synergistic cancer therapy

ABSTRACT

Due to the traditional therapies of cancer inducing huge pains to patients, the non-invasive photo-guided therapies are attracting massive attentions of researchers. Herein, the intelligent-designed carbon-dots/hemin nanoplatforms (HCDs NPs) were developed, owning high-authority photo-therapy for cancer. The fluorescence resonance energy transfer (FRET) effect enhanced the photo-thermal ability of HCDs NPs, endowing the synthesized nanoplatforms with photo-dynamic property simultaneously. Therefore, the obtained HCDs NPs could achieve synergetic photo-thermal and photo-dynamic therapies for cancer. Basing on the experimental results, the prepared HCDs NPs could induce the temperature enhancement high to ca 26 °C under laser irradiation, also with the outstanding photo-dynamic efficacy. More than 90% of cancer cells die after 10 min laser treatment. Thus, the dual-modal photo-therapeutic HCDs NPs are promising and excellent nanomaterials for potential application in synergistic cancer therapy.

1. Introduction

Traditional cancer therapies such as chemo, surgical, and radiation therapies with the defects of serious side effects, huge invasion, and low selectivity induce great pains to patients suffering from cancer, which lead to abortive cancer therapy [1,2]. In order to overcome those challenges, scientists explore many methods containing photo-dynamic [3], photo-thermal [3], gene [4], and gamma knife therapies [5], enhancing the effect of cancer therapy. Especially, photo-dynamic therapy (PDT) and photo-thermal therapy (PTT) are two remarkable non-invasive avenues which could convert the irradiating light to $^1O_2$ (cytotoxic singlet oxygen) (or ROS (reactive oxygen species)) and heat respectively, inducing local apoptosis of cancer cells [6]. Moreover, thermal effects of PTT at an appropriate level could increase available intratumoral blood flow transporting more oxygen into tumor, which cause the enhanced PDT efficacy and synergetic effect [7]. However, commercial photo-thermal agents and photo-dynamic sensitizers such as porphyrin [8], phthalocyanine [9], hypocrellin [10], methylthionine chloride [11], and indocyanine green etc. [12], possess extremely low solubility in water, easy aggregation, weak targeting to cancer cells, and single function, hindering the potential application in the field of photo-induced cancer therapy.

For further solving above-mentioned problems, researchers have developed miscellaneous multifunctional nanosystems to cure cancer effectively [13]. For instance, the chlorin e6 conjugated poly(dopamine) nanospheres possessed dual-modal therapeutic property, achieving high-effective PDT under 650 nm laser irradiation and PTT under 808 nm laser irradiation individually [14]. However, the obtained nanospheres could be irradiated by single 650 or 808 nm laser to perform PDT or PTT respectively, which induce insufficient utilization of the used laser in cancer therapy. Recently, lanthanide (Ln)-doped upconversion nanoparticles (UCNPs) have attracted considerable attention due to the ability of converting the low-energy near-infrared (NIR) light into the higher-energy [15]. The UCNPs act as the light transducers and activate the nearby photosensitizers through a fluorescence resonance energy transfer (FRET) effect process resulting in effective PDT under NIR light [16]. The metal cytotoxicity and rare species of UCNPs limit their further application in cancer therapy [17].

The emerging fluorescent carbon-dots (CDs) with upconversion ability bring new hope for UCNPs induced cancer therapy [18]. As a novel member in the family of carbon nanomaterials, CDs are widely used in the application of bioimaging [19], drug delivery [20], PTT [11], and PDT etc. [21] Protoporphyrin IX conjugated CDs have been developed and utilized for PDT successfully by the FRET efficacy between CDs and protoporphyrin IX [22]. However, the single function of the obtained nanocomposites with low efficiency of light utilization is

* Corresponding authors.
E-mail addresses: zhengyang8402@qq.com (Z. Yang), shenglq@fync.edu.cn (L. Sheng).

https://doi.org/10.1016/j.jinorgbio.2019.01.018
Received 28 October 2018; Received in revised form 17 January 2019; Accepted 31 January 2019
Available online 01 February 2019
0162-0134/

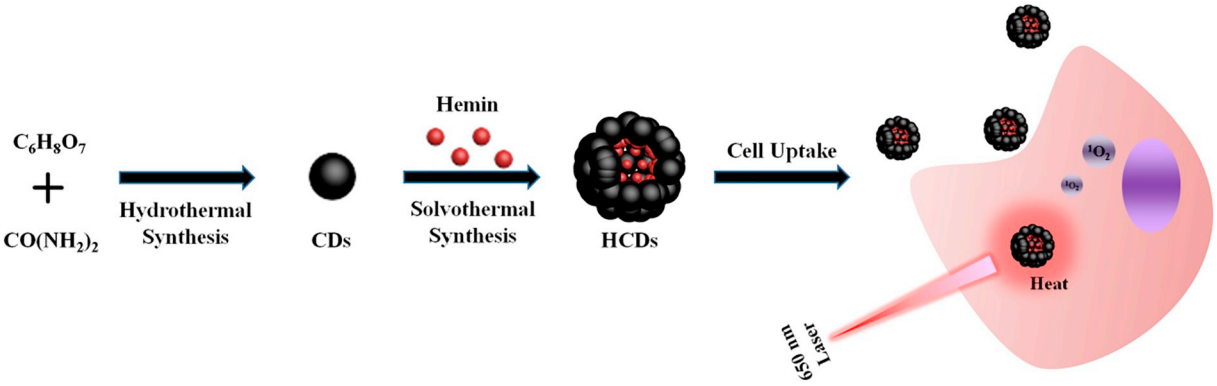

Fig. 1. Synthetic scheme and simulating response of HCDs NPs.

the key barrier weakening the potential for cancer therapy. Hemin is an important anti-cancer agent which could be accumulated by cancer cells due to the abnormal metabolism of cancer cells inducing apoptosis [23]. Researchers have reported hemin as photosensitizer which could absorb UV–Vis light ranging from 220 to 500 nm kill cancer cells rapidly by PDT [24]. But hemin could not absorb NIR light with deep tissue penetration to cure tumor in body [25].

For solving the afore-mentioned challenges in the field of cancer therapy, we developed a bi-functional nanoplatform combining with photo-thermal CDs and photosensitive hemin by facile solvothermal synthesis. The synthetic scheme and simulating response of HCDs NPs is shown in Fig. 1. The synthesized HCDs NPs not only possess FRET-enhanced photo-thermal ability, but also own FRET-induced photo-dynamic abilities simultaneously, which achieve dual-modal phototherapy for curing cancer synergistically. Moreover, the appropriate size of the obtained HCDs NPs has enhanced permeability and retention (EPR) effect, which could be accumulated through the passive targeting efficacy at tumor site. Thus, this research provides a new strategy in the domain of designing novel photo-responsive nanoplatforms for the application in the medicine and other fields. (See Table 1.)

2. Experimental section

2.1. Materials and characterization

Urea ($CO(NH_2)_2$), sodium hydroxide, dimethyl sulfoxide (DMSO) (C_2H_6OS), and citric acid were obtained from Sinopharm Chemical Reagent Co., Ltd. (China). Hydrochloric acid (36.0–38.0 wt%), hemin ($C_{34}H_{32}ClN_4O_4Fe$), and 1,3-diphenylisobenzofuran (DPBF) ($C_{20}H_{14}O$) were purchased from Sigma-Aldrich Co. LLC. 3-(4,5-dimethylthiazol-2-yl)-2,5-diphenyltetrazolium bromide (MTT), dichlorofluorescein diacetate (DCFH-DA), high glucose medium (DMEM), and pancreatin solution (25 wt%) were gained from Macklin Inc. Hoechst 33342, phosphate buffer solution (PBS), propidium iodide (PI), streptomycin, fetal bovine serum (FBS), and penicillin were obtained from Sangon Biotech Inc. All agents using in experiments were analytical pure, which were used as received without purifying further. The Mili-Q water with resistivity of 18.0 MΩ·cm was used in all experiments.

Table 1
The table of abbreviations.

Abbreviations	Complete spelling
HCDs NPs	Carbon-dots/hemin nanoplatforms
PDT	Photo-dynamic therapy
PTT	Photo-thermal therapy
UCNPs	Upconversion nanoparticles
CDs	Carbon-dots
EPR	Enhanced permeability and retention

A Via-Reflex laser confocal Raman spectroscopy was used to collect Raman spectra. The Shimadzu UV-1800 spectrophotometer and NEXUS-870 FTIR spectrometer (KBr pellet technique) were used to obtain UV–Vis and Fourier transform infrared (FT-IR) spectra, respectively. DX-2700 X-ray diffraction (XRD) was used to analyse the crystallinity of samples by collecting the powder X-ray diffraction (XRD) patterns (CuKα radiation, λ = 1.54056 Å, 40 V, 100 mA, 6°/min). Fluke Ti32 infrared thermography camera was used to evaluate the photothermal effects of water, CDs, and HCDs NPs by acquiring the thermographies. The morphological details of the obtained samples were studied by Transmission electron microscopy (TEM) (JEM 100SX, 200 kV) and Field emission scanning electron microscopy (FE-SEM) (SU 1510, 10 kV). The zeta potentials and size distributions of all samples were obtained using laser Doppler electrophoretic methods and dynamic light scattering (DLS) of Malvern zetasizer nano (UK) respectively.

2.2. Preparation of CDs

In general, 1.0 g of citric acid and 0.7 g of urea were added into 30 mL of pure water. After 30 min sonication, the mixed solution sealing in a 50 mL Teflon-lined stainless autoclave was heated to 150 °C maintaining for 5 h. Till the autoclave was cooled down naturally, the acquired dispersion was dialyzed against pure water overnight in a dialysis bag with MWCO (molecular weight cutoff) 3.5 kDa. At last, the dialyzing dispersion with 10 min refrigeration at −86 °C was followed by the process of freeze-drying to produce powdery CDs with the color of black-green.

2.3. Preparation of HCDs NPs

CDs aqueous dispersion (1 mL) with the concentration of 5 mg·mL^{-1} and hemin (50 mg) were added into DMSO (20 mL) followed by 30 min sonication. Then, the mixed suspension sealing in a 50 mL Teflon-lined stainless autoclave was heated to 160 °C and maintained for 6 h. Till the obtained dark-black dispersion was cooled down to environmental temperature, the acquired dispersion was dialyzed against NaOH solution (0.01 M) firstly by a dialysis bag with MWCO 3.5 kDa over 24 h, removing the residual free hemin and DMSO. Subsequently, the dialyzed suspension was further subjected to a dialysis against deionized water using a dialysis membrane with MWCO 3.5 kDa over 24 h. Finally, the dark-black powders of HCDs NPs were obtained by freeze-drying.

2.4. MTT assay

The obtained CDs and HCDs NPs were prepared to dispersions with different concentrations (0.1, 0.5, and 1 mg·mL^{-1}, respectively) by DMEM medium. The cell line of human hepatocellular carcinoma

(HepG2) was suspended in DMEM medium and seeded into 96-well plates at a density of 5×10^3 per well (200 μL). After 24 h incubation, each well was washed by PBS for three times. Then pure medium (100 μL, as control), CDs containing, and HCD NPs containing medium (0.1, 0.5, and 1 mg·mL^{-1}, respectively) (100 μL) were added to different wells with further incubation for 24 h. Subsequently, the old medium was removed by PBS, following by the addition of MTT (20 μL) and DMEM medium (100 μL) to each well, incubating for another 4 h. For comparison, the irradiated groups were irradiated by a 650 nm laser for 10 min, further incubating over 24 h. The optical density of all groups was measured after the addition of DMSO solution (100 μL) for dissolving the insoluble formazan crystals by an Elisa reader at 490 nm.

2.5. Intracellular ROS determination

HepG2 cells were seeded into 6-well plates at a density of 5×10^4 per well (1 mL) with incubation over 24 h. The CDs and HCDs NPs (0.1 mg·mL^{-1}) containing medium were used to treat all cells respectively after removing the old medium. With further 6 h incubation, the cells were washed by PBS for 3 times, following by treating all groups with DCFH-DA (10 μmol·L^{-1}) over 50 min at 37 °C. The illumination groups were irradiated under a 650 nm laser for 3 min. Then all groups were rinsed with PBS for three times. Due to the DCFH could be oxidized to 2,7-dichloro-fluorescein (DCF) by hydroxyl (·OH) radicals, the strong fluorescence would be observed demonstrating the generation of intracellular ROS. The detection of $^1O_2$ was measured by the same way.

2.6. Fluorescent images

To further study the cytotoxicity of CDs and HCDs NPs, fluorescence dyes (Hoechst 33342 and PI) were used for assessing the apoptosis of HepG2 cells. In general, HepG2 cells were seeded into 12-well plates at a density of 5×10^4 per well, incubating at 37 °C under 5% CO_2 atmosphere over 24 h. Then CDs and HCDs NPs containing medium (0.5 mg·mL^{-1}) were added to selected wells respectively, following by dark incubation for 24 h. During the incubation, the illumination groups were irradiated by a 650 nm laser for 10 min with further incubation till to 24 h. Subsequently, PBS was used to remove the old medium, following by the addition of Hoechst 33342 (0.5 mL, 10 μg·mL^{-1}) and PI (0.5 mL, 10 μg·mL^{-1}) to each well staining for 15 min respectively. Finally, the cells were washed by PBS for 4 times, and the corresponding fluorescent images were collected by an inverted fluorescence microscopy.

3. Results and discussion

3.1. Morphology and structure of HCDs NPs

For the morphological characterizations of CDs and HCDs NPs, TEM and SEM images were collected (Fig. 2). In Fig. 2a, the CDs are nanodots possessing the average diameters about 3 nm, which prove the CDs possess ultra-small size and good dispersity. From Fig. 2b, the obtained HCDs NPs own spherical structure with the symmetrical diameters ranging from 80 to 100 nm, which are corresponding to the results in Fig. 2c. The size of HCDs NPs enlarged obviously comparing to that of CDs, which may be caused by that the hemin conjugated CDs graft by self-assembly to form spherical nanoplatforms during the dialysis process. The aforementioned evidences indicate that the prepared HCDs NPs possess suitable size contributing to EPR at tumor site.

FT-IR spectra of different samples were obtained and shown in Fig. 3A. According to Fig. 3A-a, the strong peak at 1570 cm^{-1} and the broad peak at 3420 cm^{-1}are assigned to the bending vibration and stretching vibration of NH respectively, proving large amounts of amino group in CDs. Meanwhile, the peaks at 3200, 1400, and 1200 cm^{-1} are corresponded to the stretching vibration, bending vibration, and scissoring vibration of C—OH, OH, and C—OH, respectively. Furthermore, the peaks at 1128 and 1670 cm^{-1} are ascribed to the asymmetrical stretching vibration and stretching vibration of C—NH—C and C═O respectively. The aforementioned proofs demonstrate the substantial existence of carboxyl and amino groups in the synthesized CDs [26]. As shown in Fig. 3A-c, the peaks of HCDs NPs at 1570 and 3200 cm^{-1} present weakened-intensities comparing to those of CDs, due to the amidation between CDs and hemin. Furthermore, the peak intensity of C═O vibration in HCDs NPs at 1640 cm^{-1} enhance obviously, indicating more content of C═O than that of hemin in Fig. 3A-b. Moreover, the new peaks at 966, 2920, and 2870 cm^{-1} in Fig. 3A-c are corresponded to characteristic signal of pyrrole structure and C—H stretching vibration, which are induced by the grafting hemin in HCDs NPs [27]. The same evidences coming from enlarged FT-IR spectra of all samples (Fig. S1) also demonstrate that the prepared HCDs NP are combined by hemin and CDs successfully.

The qualitative characteristics of CDs and HCDs NPs were evaluated by Raman spectra (Fig. 3B). Both samples exhibit two major characteristic peaks of D and G band around at 1385 and 1580 cm^{-1}, respectively [28]. The peak intensity of HCDs NPs at 1385 cm^{-1} (Fig. 3B-b) is higher than that of CDs (Fig. 3B-a), demonstrating the more disordered carbon in the structure of HCDs NPs. The phenomenon may be due to the increased edge defects of HCDs NPs by hemin grafting.

UV–Vis spectra were used (Fig. 3C) for the investigation of the optical properties of CDs, hemin, and HCDs NPs respectively. The obtained HCDs NPs (Curve c) possess the characteristic peak at 339 nm, which is corresponding to that of CDs (Curve a), indicating the existence of C═O. Meanwhile, the spectrum of hemin (Curve b) shows a Soret peak at 388 nm as well as a weak peak around 630 nm. After the combination of hemin and CDs, the prepared HCDs NPs also show the Soret peak at 395 nm. Comparing to monomeric hemin, the peak occurs a little red shift, which may be induced by the amidation of CDs and hemin [29]. The enlarged visible spectrum of HCDs NPs in insert exhibits wide absorption band ranging from 550 to 690 nm, which is attributed to the grafted hemin, demonstrating the HCDs NPs could absorb the light with the wavelength around 650 nm effectively. Therefore, the above-mentioned analysis illustrates HCDs NPs are synthesized by the combination of hemin and CDs successfully, possessing huge potential in the application of phototherapy for cancer.

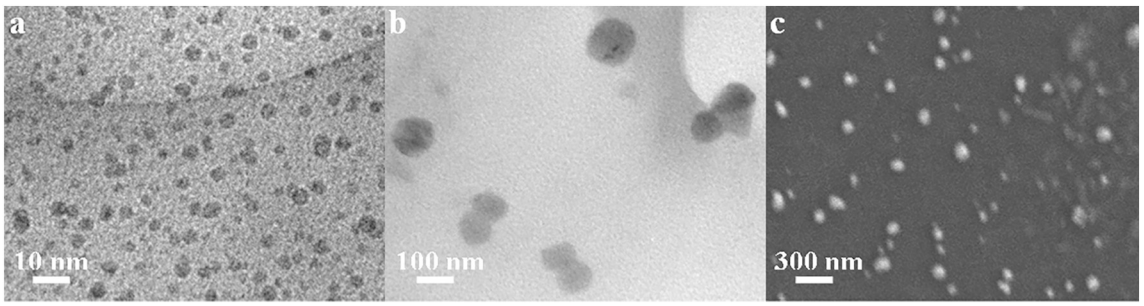

Fig. 2. TEM images of (a) CDs and (b) HCDs NPs, respectively; and SEM image of (c) HCDs NPs.

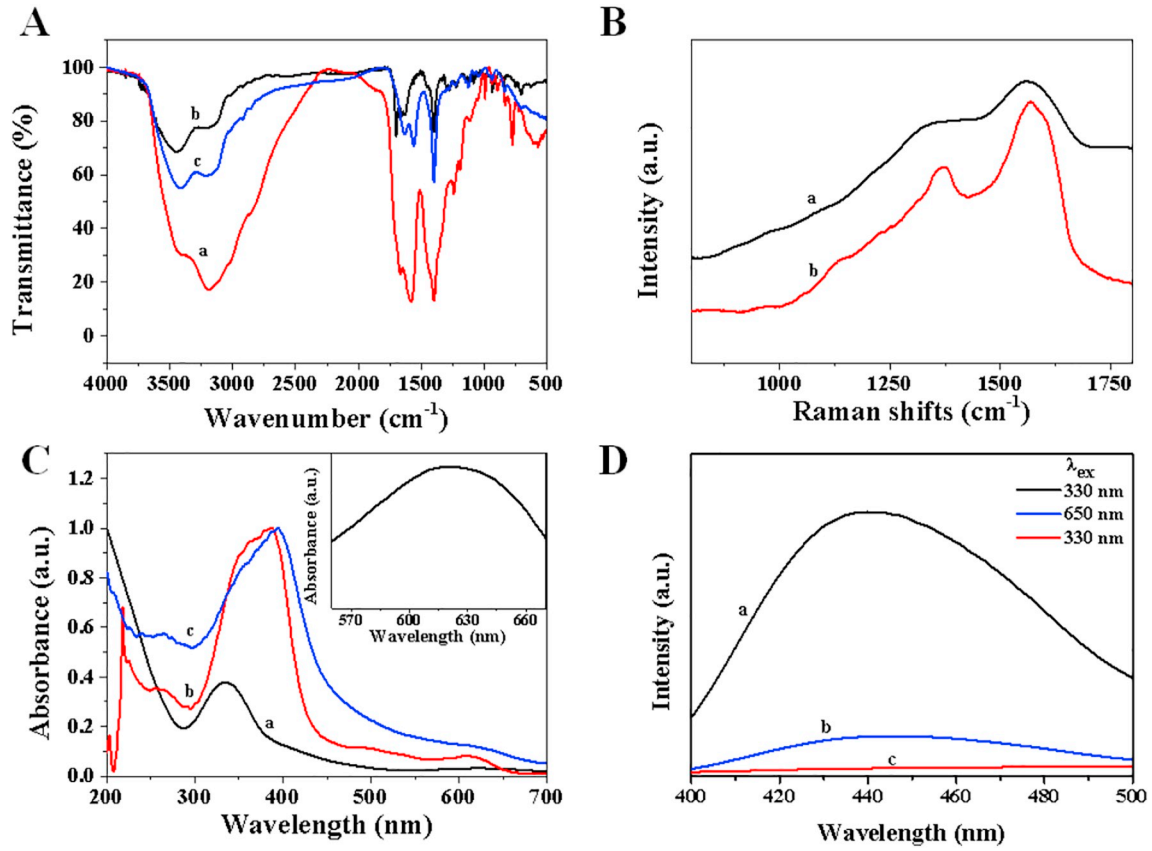

Fig. 3. (A) FT-IR spectra of (a) CDs, (b) hemin, and (c) HCDs NPs, respectively; (C) Raman spectra of (a) CDs and (b) HCDs NPs; (C) UV–Vis spectra of (a) CDs, (b) hemin, and (c) HCDs NPs, respectively (the enlarged visible spectrum in insert shows the absorption of obtained HCDs NPs ranging from 550 to 690 nm); and (D) Fluorescent emission spectra of (a) CDs, (b) up-conversion of CDs, and (c) HCDs NPs.

For further investigation, fluorescence spectra of CDs (Fig. 3D-a) and HCDs NPs (Fig. 3D-c) were collected to study the FRET efficacy between CDs and hemin in the structure of HCDs NPs respectively. Accompany with the excitation at 330 nm, a strong emission peak of CDs around 440 nm is observed. Meanwhile, the up-converted fluorescence (Fig. 3D-b) of CDs with the weak emission peak (440 nm) which is excited at 650 nm indicates the CDs possess excellent up-convertible ability. However, HCDs NPs show negligible fluorescence with the excitation at 330 nm, illustrating the fluorescence is quenched due to the integration of CDs and hemin. According to Fig. 3C, both CDs and hemin could absorb the blue fluorescence around the peak at ca. 440 nm effectively. Therefore, the self-quenching phenomenon of HCDs NPs occurs due to the FRET efficacy from CDs to CDs, enhancing the photo-thermal effect of the prepared HCDs NPs [30]. Furthermore, the FRET efficacy from CDs to hemin contributes the photo-dynamic property of hemin too, causing strengthened photo-dynamic effect of the prepared HCDs NPs [11]. Thus, the photo-thermal and photo-dynamic properties of the synthesized HCDs NPs are strengthened simultaneously, which are mainly attributed to the smart design for combining CDs and hemin, causing the enhanced FRET efficacy in the obtained HCDs NPs.

For studying the size distributions of HCDs NPs, DLS measurements of HCDs NPs were performed in physiological environments such as PBS, serum-free medium, and serum-containing medium respectively (shown in Fig. 4a). The average diameters of the HCDs NPs in PBS, serum-free medium, and serum-containing medium of ca. 107, 123, and 135 nm respectively are consistent with that from the TEM images. Therefore, the HCDs NPs possess good stability in physiological environments without any clear aggregation.

For further investigation of the dispersivity of synthesized HCDs NPs, zeta potentials of HCDs NPs in PBS, serum-free medium, and serum-containing medium were obtained respectively, simulating the physiological environments (Fig. 4B). The measured mean zeta potentials of the HCDs NPs are ca −33, −38, and −46 mV respectively, demonstrating the prepared HCDs NPs possess good dispersivity in different dispersions simulating the physiological environments.

The photo-thermal effects of all samples were investigated in Fig. 4C. Under continuous irradiation of 650 nm laser for 10 min, the temperature elevation of CDs dispersion (1 mg·mL^{-1}) increases about 6 °C. However, the temperature enhancement of water is ignorable. For comparison, the irradiated HCDs NPs dispersions (0.1, 0.5, and 1 mg·mL^{-1}) emerge remarkable temperature changes with the enhancements about 26, 25, and 27 °C respectively, which are remarkably higher than those of other samples. The enhanced photo-thermal effect of HCDs NPs may be due to the quenched fluorescence of CDs which is induced by the FRET effect [31]. The abovementioned evidences demonstrate the synthesized HCDs NPs possessing excellent photo-thermal performance, which could be used in PTT of cancer as a novel photo-thermal agent.

For further understanding photo-dynamic efficacy of the HCDs NPs, DPBF and HCDs NPs mixed dispersion was irradiated by a 650 nm laser for 10 min to detect the generation $^1O_2$ (ROS). The results in Fig. 4D show that the intensity of characteristic peak of DPBF at 410 nm remarkably decline after the 10 min laser irradiation. Meanwhile, the DPBF solution in water is irradiated by 650 nm laser for 10 min, which the characteristic peak at 410 nm decline extremely weak (Fig. S2), demonstrating that only laser irradiation could not induce photo-dynamic effect in DPBF solution. In addition, the intensity of which has negligible changes without irradiation in the same time, demonstrating the prepared HCDs NPs are efficacious photo-dynamic agents, possessing potential application in PDT of cancer. The photo-dynamic mechanism of the HCDs NPs is attributed to the FRET effect between CDs

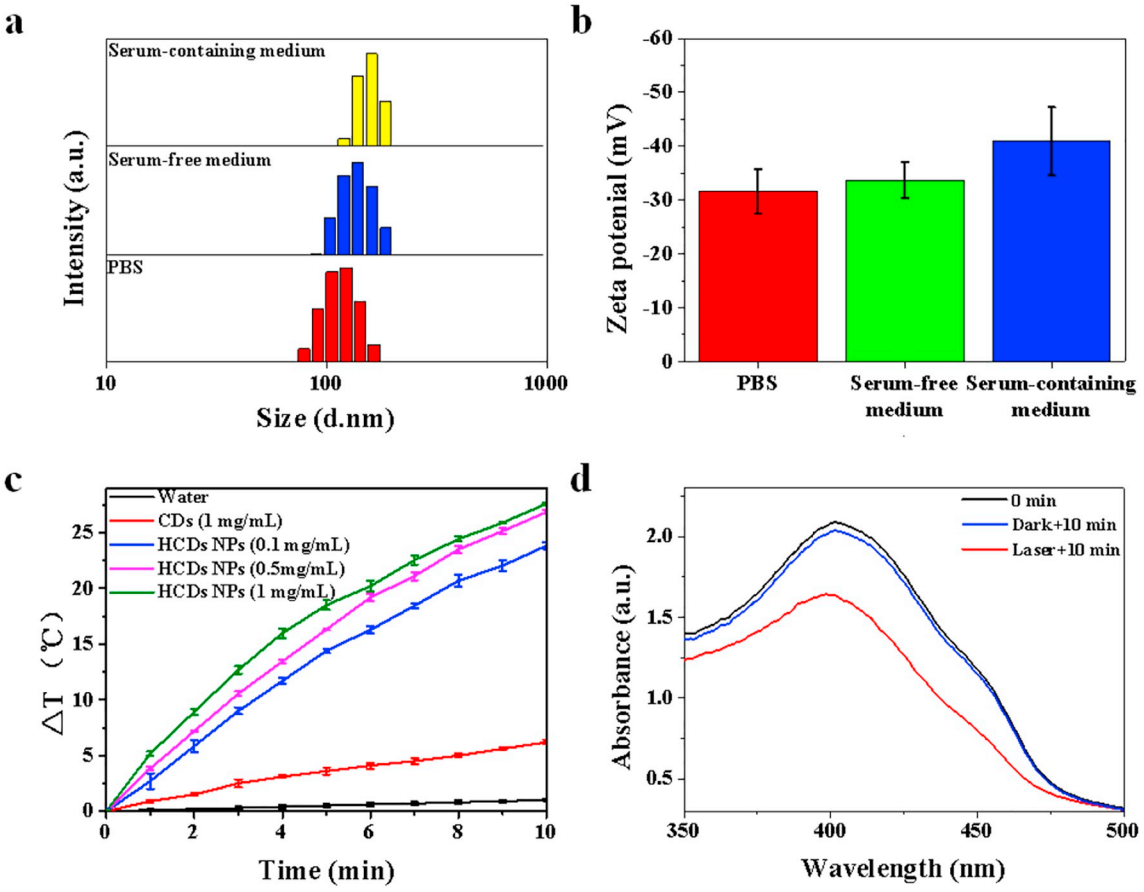

Fig. 4. (A) Size distributions and (B) Zeta potentials of HCDs NPs in PBS, serum-free medium, and serum-containing medium respectively, simulating the physiological environments; (C) Photo-thermal effects of water, the dispersion of CDs and HCDs NPs with different concentration respectively; (D) Photo-dynamic effect of HCDs NPs.

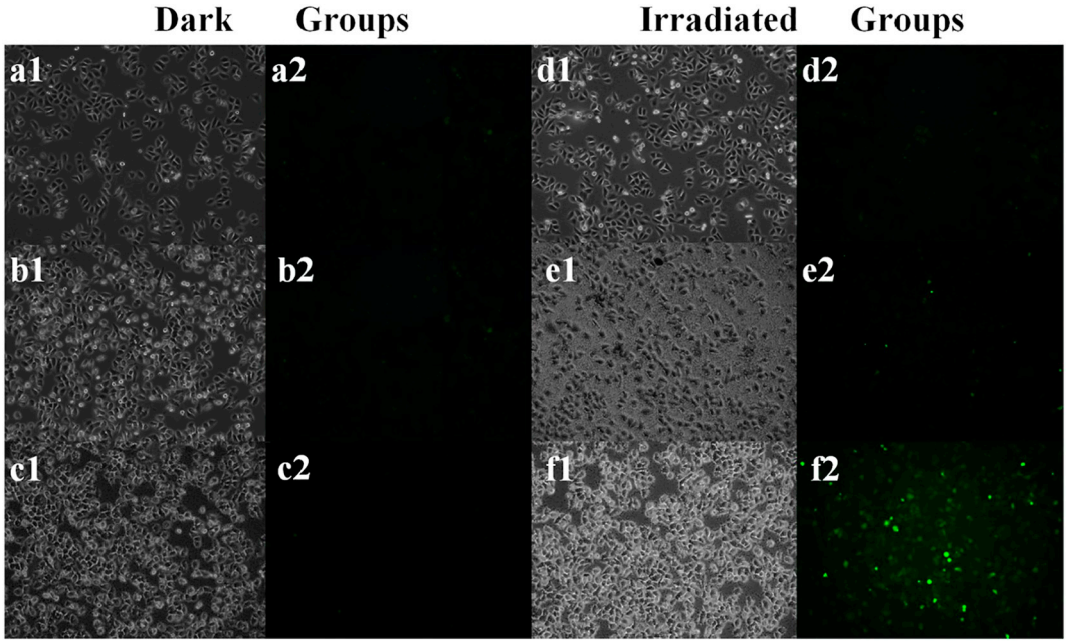

Fig. 5. Bright-field and fluorescence microscopy images of HepG2 cells incubated with (a, d) Control groups (without samples), (b, e) CDs, and (c, f) HCDs NPs (a–c) without laser irradiation and (d-f) with laser irradiation (650 nm, 1 W·cm^{-2}), respectively. All groups were treated with DCFH-DA (10 μmol·L^{-1}) at 37 °C for 50 min before irradiation.

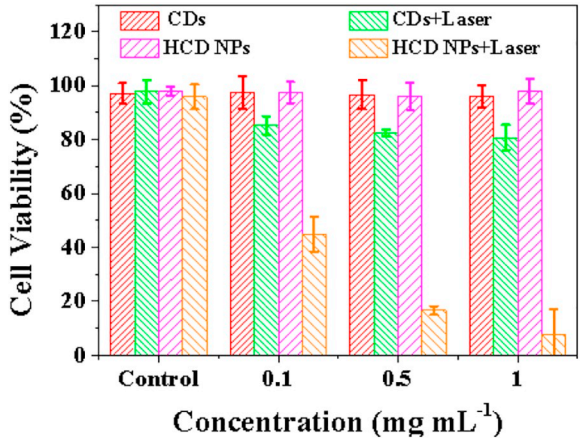

Fig. 6. Cytotoxicity assay of HepG2 cells incubated with various concentrations of CDs and HCDs NPs without and with laser irradiation.

and hemin in the synthesized nanoplatforms [32]. All aforementioned results illustrate that the obtained HCDs NPs possess significant photo-convertible property inducing simultaneous photo-thermal and photo-dynamic efficacies.

3.2. Intracellular ROS determination

As shown in Fig. 5, to study the generation of intracellular ROS, DCFH-DA was used to treat HepG2 cells with different samples [11]. Fig. 5a2–c2 exhibits no green fluorescence from HepG2 cells with the co-incubation of PBS, CDs, and HCDs NPs, demonstrating that all groups in dark could not engender intracellular ROS. Fig. 5d2 and e2 shows negligible fluorescence indicating PBS and CDs co-incubated HepG2 cells with laser irradiation could not induce intracellular ROS. However, the group of HCDs NPs irradiating by laser exhibits the bright green fluorescence in Fig. 5f2, illustrating that large amounts of ROS are induced in HepG2 cells. The abovementioned results prove that HCDs NPs are high-performance photo-dynamic photosensitizers inducing the generation of ROS in cancer cells, which are advantageous to phototherapy of cancer.

3.3. MTT assay

For further studying the phototherapy efficacies of CDs and HCDs NPs, MTT assay was used to evaluate the cytotoxicity of CDs and HCDs NPs with or without laser irradiation (Fig. 6). The control groups are incubated without any samples which show the cell viabilities all above 90% with or without laser irradiation, demonstrating the growth of cancer cells could not be affected by laser irradiation. Meanwhile, the co-incubated groups of CDs and HCDs NPs with various concentrations 0.1, 0.5, and 1 mg·mL^{-1} respectively were divided into non-irradiated groups or irradiated groups, individually. All the non-irradiated groups exhibit that the cell viabilities are above 90%, demonstrating there are no clear cytotoxicity of CDs and HCDs NPs, also indicating HCDs NPs have good biocompatibility. Moreover, the irradiated groups of CDs exhibit few decrease of the cell viabilities, which illustrates the CDs have limited photo-thermal ability for killing cancer cells. However, the co-incubated groups of HCDs NPs with laser irradiation exhibit remarkable cytotoxicity with the cell viabilities of ca. 44.83%, 16.61%, and 7.73% at the concentrations of 0.1, 0.5, as well as 1 mg·mL^{-1}, respectively. The main reason is that the HCDs NPs not only have the excellent photo-thermal effect, but also own hemin-endowed photo-dynamic property, achieving synergistic photo-thermal and photo-dynamic therapies. Thus, the prepared HCDs NPs are high-authority photo-therapeutic agents, possessing dual-modal synergetic photo-therapies.

3.4. Fluorescent imaging

As shown in Fig. 7, the groups of control, CDs, and HCDs NPs co-incubated HepG2 cells without laser irradiation emit blue fluorescence (a1–c1) as well as negligible red fluorescence (a2–c2), respectively. The results demonstrate all the cells grow well without apparent cell apoptosis. Meanwhile, the group of control with laser irradiation shows blue fluorescence (d1) and minimal red fluorescence (d2), illustrating the apoptosis of HepG2 cells could not be induced by mere laser irradiation. The group of CDs under laser irradiation also exhibits blue fluorescence (e1) and indistinct red fluorescence (e2), demonstrating the CDs based photo-thermal effect could not effectively induce cancer cell death. After HCDs NPs co-incubated cells are exposed under laser irradiation within 10 min, the strong red fluorescence in the merged image (f3) could be seen, which show the phototherapy efficacy of HCDs NPs causing massive cell death [31]. Thus, the HCDs NPs are

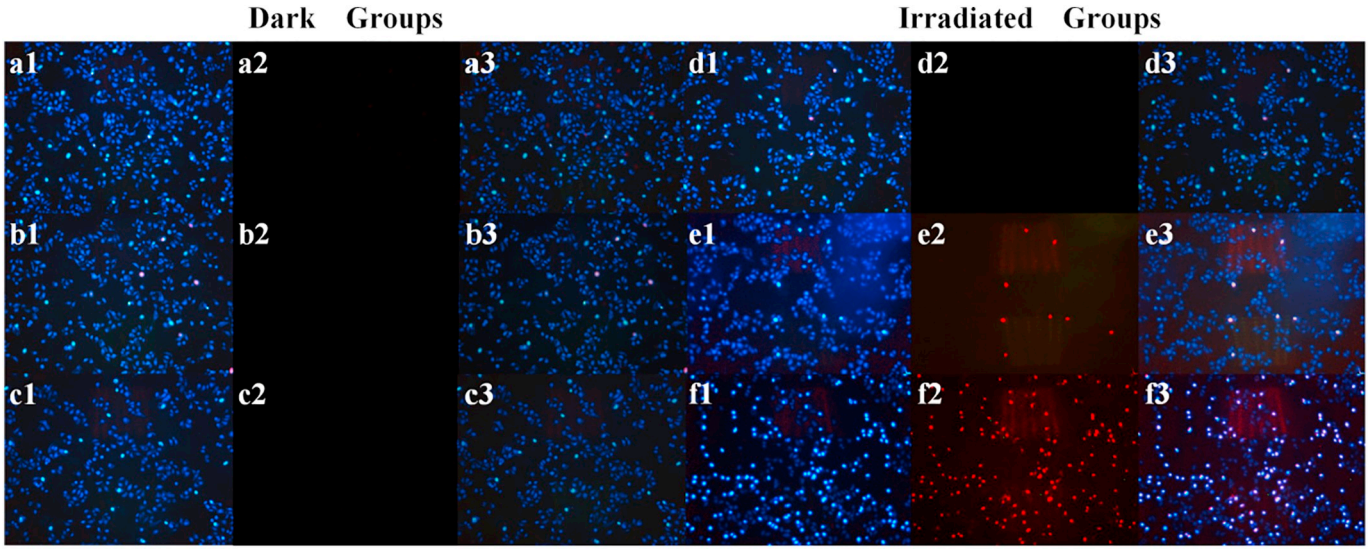

Fig. 7. Fluorescence microscopy images of Hoechst 33342/PI-stained HepG2 cells co-incubated with (a) Control (without samples), (b) CDs and (c) HCDs NPs without laser irradiation, and (d–f) the corresponding groups under laser irradiation for 10 min (650 nm, 1 W·cm^{-2}).

novel dual-modal photo-responsive agents with excellent synergetic abilities for photo-thermal and photo-dynamic therapies.

4. Conclusion

To sum up, novel HCDs NPs were synthesized by facile solvothermal method. According to the experimental results, the obtained HCDs NPs own good biocompatibility and suitable size, which are advantageous to apply in the biomedical field. The prepared HCDs NPs with the smart design possess high-performance photo-convertibility through the FRET effect. The therapeutic NIR laser could be converted to photo-thermal and photo-dynamic efficacies by HCDs NPs synchronously, achieving synergistic PTT and PDT in cancer therapy. This study provides a new strategy to design and synthesize other multi-functional nanoplatforms for cancer therapy.

Acknowledgements

This work is supported by the Anhui Province Foundation of China (GXBJZD21) and Fuyang City Foundation (HDHX2016009).

Appendix A. Supplementary data

Supplementary data to this article can be found online at https://doi.org/10.1016/j.jinorgbio.2019.01.018.

References

[1] J.M. Brown, A.J. Giaccia, Cancer Res. 58 (1998) 1408–1416.
[2] J. Bourhis, J. Overgaard, H. Audry, K.K. Ang, M. Saunders, J. Bernier, J.-C. Horiot, A. Le Maître, T.F. Pajak, M.G. Poulsen, B. O'Sullivan, W. Dobrowsky, A. Hliniak, K. Skladowski, J.H. Hay, L.H.J. Pinto, C. Fallai, K.K. Fu, R. Sylvester, J.-P. Pignon, Lancet 368 (2006) 843–854.
[3] E.S. Shibu, M. Hamada, N. Murase, V. Biju, J Photochem Photobiol C: Photochem Rev 15 (2013) 53–72.
[4] L. Xu, T. Anchordoquy, J. Pharm. Sci. Technol. 100 (2011) 38–52.
[5] A.M. Faramand, H. Kano, S. Johnson, A. Niranjan, J.C. Flickinger, L.D. Lunsford, Am. J. Neuroradiol. 39 (2018) 1907–1911.
[6] D.F. Costa, L.P. Mendes, V.P. Torchilin, Adv. Drug Deliv. Rev. 133 (2018) 95–116.
[7] G. Tian, X. Zhang, Z. Gu, Y. Zhao, Adv. Mater. 27 (2015) 7692–7712.
[8] L. Cheng, A. Kamkaew, H. Sun, D. Jiang, H.F. Valdovinos, H. Gong, C.G. England, S. Goel, T.E. Barnhart, W. Cai, ACS Nano 10 (2016) 7721–7730.
[9] G. Obaid, I. Chambrier, M.J. Cook, D.A. Russell, Angew. Chem. Int. Ed. 51 (2012) 6158–6162.
[10] J.-E. Chang, H.-J. Cho, E. Yi, D.-D. Kim, S. Jheon, J. Photochem. Photobiol. B Biol. 158 (2016) 113–121.
[11] Z. Liu, W. Chen, Y. Li, Q. Xu, Anal. Chem. 88 (2016) 11955–11962.
[12] S.M. Sharker, J.E. Lee, S.H. Kim, J.H. Jeong, I, in: H. Lee, S.Y. Park (Eds.), Biom, vol. 61, 2015, pp. 229–238.
[13] L. Han, C. Tang, C. Yin, ACS Appl. Mater. Interfaces 8 (2016) 23498–23508.
[14] D. Zhang, M. Wu, Y. Zeng, L. Wu, Q. Wang, X. Han, X. Liu, J. Liu, ACS Appl. Mater. Interfaces 7 (2015) 8176–8187.
[15] X. Liu, C.-H. Yan, J.A. Capobianco, Chem. Sci. Rev. 44 (2015) 1299–1301.
[16] N.M. Idris, M.K.G. Jayakumar, A. Bansal, Y. Zhang, Chem. Sci. Rev. 44 (2015) 1449–1478.
[17] A.E. Guller, A.N. Generalova, E.V. Petersen, A.V. Nechaev, I.A. Trusova, N.N. Landyshev, A. Nadort, E.A. Grebenik, S.M. Deyev, A.B. Shekhter, A.V. Zvyagin, Nano Res. 8 (2015) 1546–1562.
[18] N. Durán, M.B. Simões, A.C.M. de Moraes, W.J. Fávaro, A.B. Seabra, J. Biomed. Nanotechnol. 12 (2016) 1323–1347.
[19] M. Ghosh, S.K. Sonkar, M. Saxena, S. Sarkar, Small 7 (2011) 3170–3177.
[20] N. Gogoi, D. Chowdhury, J. Mater. Chem. B 2 (2014) 4089–4099.
[21] J. Ge, Q. Jia, W. Liu, L. Guo, Q. Liu, M. Lan, H. Zhang, X. Meng, P. Wang, Adv. Mater. 27 (2015) 4169–4177.
[22] C. Fowley, N. Nomikou, A.P. McHale, B. McCaughan, J.F. Callan, Chem. Commun. 49 (2013) 8934–8936.
[23] J.C. Kennedy, R.H. Pottier, J. Photochem. Photobiol. B Biol. 14 (1992) 275–292.
[24] Q. Yu, A. Xie, Y. Xiao, S. Li, F. Huang, Y. Shen, J. Mater. Chem. B 3 (2015) 1439–1445.
[25] D. Jaque, L. Martínez Maestro, B. del Rosal, P. Haro-Gonzalez, A. Benayas, J.L. Plaza, E. Martín Rodríguez, J. García Solé, Nanoscale 6 (2014) 9494–9530.
[26] R. Qu, L. Shen, Z. Chai, C. Jing, Y. Zhang, Y. An, L. Shi, ACS Appl. Mater. Interfaces 6 (2014) 19207–19216.
[27] S. Pandey, M. Thakur, A. Mewada, D. Anjarlekar, N. Mishra, M. Sharon, J. Mater. Chem. B 1 (2013) 4972–4982.
[28] A. Pal, M.P. Sk, A. Chattopadhyay, ACS Appl. Mater. Interfaces 8 (2016) 5758–5762.
[29] T. Feng, X. Ai, G. An, P. Yang, Y. Zhao, vol. 10, ACS Nano (2016) 4410–4420 (Am. Chem. Soc. 10).
[30] C. Urban, A.S. Urban, H. Charron, A. Joshi, Trans. Cancer Res. 2 (2013) 292–308.
[31] M. Guo, J. Huang, Y. Deng, H. Shen, Y. Ma, M. Zhang, A. Zhu, Y. Li, H. Hui, Y. Wang, X. Yang, Z. Zhang, H. Chen, Adv. Funct. Mater. 25 (2015) 59–67.
[32] J. Wang, Z. Zhang, S. Zha, Y. Zhu, P. Wu, B. Ehrenberg, J.Y. Chen, Biomaterials 35 (2014) 9372–9381.